Journal of Alloys and Compounds 566 (2013) 31–36

Contents lists available at SciVerse ScienceDirect

Journal of Alloys and Compounds

journal homepage: www.elsevier.com/locate/jalcom

Induced magnetic anisotropy features in FeCrSiBNbCu nanocrystalline alloy: Role of stress distribution proven by direct X-ray measurements

G.V. Kurlyandskaya [a,b,*], V.A. Lukshina [c], A. Larrañaga [d], I. Orue [d], A.A. Zaharova [b,c], D.A. Shishkin [b,c]

[a] Department of Electricity and Electronics, University of Basque Country UPV-EHU, Box 644, 48080 Bilbao, Spain
[b] Urals Federal University, Lenin St. 51, 620000 Ekaterinburg, Russia
[c] Institute of Metal Physics UD RAS, 620990 Ekaterinburg, Russia
[d] SGIker, University of Basque Country UPV-EHU, Box 644, 48080 Bilbao, Spain

ARTICLE INFO

Article history:
Received 28 February 2013
Accepted 2 March 2013
Available online 14 March 2013

Keywords:
Nanocrystalline Fe-based soft magnetic materials
Stress-induced magnetic anisotropy
X-ray diffraction
Magnetization process

ABSTRACT

$Fe_{73.5-x}Cr_xSi_{13.5}B_9Nb_3Cu_1$ ($x = 1$, 2, and 3) amorphous ribbons were prepared by single roller rapid quenching technique. Both conventional and stress annealing at 520 °C for 2 h at the value of the specific load of 150 MPa resulted in the formation of a nanocrystalline structure with average grain size about 13 nm. No significant differences in crystallite size were observed for all samples under consideration. The crystallite orientations were practically isotropic indicating no texture in the samples of all types. For all conventionally annealed ribbons a longitudinal effective magnetic anisotropy with an easy magnetization axis parallel to the ribbon axis was observed. For all stress annealed ribbons a transverse induced magnetic anisotropy with the anisotropy constant value of about 1800 ± 50 J/m^3 was evident. Induced magnetic anisotropy features in FeCrSiBNbCu nanocrystalline alloy, namely an importance of the stress distribution was proven by direct X-ray measurements. A very good correlation between the induced magnetic anisotropy constant values and anisotropic stress distribution was observed.

1. Introduction

In the last three decades, iron-based nanostructured soft ferromagnetic alloys have attracted huge attention, both for fundamental research and technological applications because of their unusual structural, electrical, magnetic, optical properties, and their resistance to corrosion [1–3]. In particular, the structure, magnetic properties and magnetoimpedance of the so-called classic FINEMET ($Fe_{73.5}Si_{13.5}B_9Nb_3Cu_1$ soft ferromagnetic alloy characterized by high values of saturation polarization and magnetoimpedance, low values for the coercive force and core losses) have been the most widely studied [4–6]. Recently, new alloys based on the classic FINEMET were created by changing the composition. For example, it was shown [7,8] that the addition of chromium and iron reduction compared to with the classic FINEMET led to an increase in the temperature of crystallization and an increase in the resistance to corrosion of the alloys.

The excellent soft magnetic properties of FINEMETs are based on the two ferromagnetic phases of the microstructure consisting of nanocrystalline grains (typically with an average size of about 10 nm) surrounded by an amorphous matrix. In order to obtain optimal structure and properties, amorphous precursors are generally annealed at temperatures above the primary crystallization temperature of approximately 510 °C [9]. Induced anisotropy was shown to be a special tool in tailoring magnetic responses making it possible to tune the magnetic permeability by stress of field annealing [3,9,10]. In stress annealed FINEMET alloys unidirectional pair ordering and magnetoelastic coupling were discussed as the origin of the induced magnetic anisotropy [11–14]. For example, Kernion et al. [14] came to the conclusion that magnetoelastic coupling is the primary source of anisotropy as originally proposed for FINEMET alloys by Herzer [12]. Direct evidence of structural origin of strain-induced magnetic anisotropy in FeSiBNbCu nanocrystalline alloys was discussed by Ohnuma et al. [15]. They found direct indication that the spacing of the (310) plane normal to the tensile direction is about 0.2% larger than the one parallel to it. This causes the distance of the iron atoms to elongate along the direction parallel to the tensile stress.

In order to understand the origin of the induced magnetic anisotropy special efforts were made to analyze the texture features in nanocrystalline FINEMET like materials after stress annealing. For many different compositions it was shown that stress annealing typically results in no texturing of the nanocrystallized material [16,17]. Recently new techniques suitable for the studies of the structure of very brittle nanocrystalline materials without

* Corresponding author at: Department of Electricity and Electronics, University of Basque Country UPV-EHU, Box 644, 48080 Bilbao, Spain. Tel.: +34 619559278; fax: +34 946013071.
E-mail address: galina@we.lc.ehu.es (G.V. Kurlyandskaya).

0925-8388/$ - see front matter © 2013 Elsevier B.V. All rights reserved.
http://dx.doi.org/10.1016/j.jallcom.2013.03.006

special preparation like spark-cut of the disks from the ribbon [16] or complex composites consisting of several overlapping layers of 5–6 mm long fragments [18] have become available.

Ohuma et al. [17] have studied the transverse magnetic anisotropy in FeSiBNbCu alloy and emphasized the importance of the magnetoelastic effect in the $Fe_{1-x}Si_x$ nanocrystals deformed during stress annealing: the effect was found to be proportional to the value of the tensile stress. However, they discussed only one reflection (the (620) for the Fe_3Si phase). Chernenkov et al. [18] filled the gap by detailed study of the structure of nanocrystalline FeSiNbCu alloy after nanocrystallization with or without load in the same "time–temperature conditions" using complex composite samples for X-ray diffraction studies in a transmission geometry. From the position of the (hkl) diffraction peak they estimated corresponding interplanar distances in the $Fe_{1-x}Si_x$ nanocrystal lattice and found that the difference of the (hkl) peaks positions in the directions of parallel and perpendicular to the ribbon axis (parallel is a direction of the application of the stress in the case of stress annealing) shows the strain of the nanocrystals in the (hkl) direction. The authors had mentioned in their work [18] that residual structure distortions should be discussed using the elastic deformation tensor, mentioning at the same time existing experimental difficulties. In a continuation of these studies (both [17,18] in a transmission mode) we propose to study the origin of magnetic anisotropy induced by stress annealing using the reflection X-ray $\mathrm{Sin}^2\psi$ technique applied to single amorphous ribbon, as opposed to the composite consisting of several overlapping layers.

In this work magnetic anisotropy, structural features and stress distribution evaluated by direct X-ray measurements are comparatively analyzed for $Fe_{73.5-x}Cr_xSi_{13.5}B_9Nb_3Cu_1$ (x = 1, 2, and 3) ribbons nanocrystallized either by conventional or stress annealing.

2. Experimental procedure

Different compositions of soft nanocrystalline materials can show distinctive features. Cr containing nanocrystalline alloys were recently attracting additional interest [8,9] due to the chromium positive influence on soft magnetic properties, increase of resistance against corrosion and increase of the thermal stability [19]. Chromium containing ribbons were also extensively studied as showing very high values of the stress induced magnetic anisotropy constant (K_u): in many cases the directional pair ordering mechanisms were associated with the presence of chromium [20]. Therefore, for present studies of nanocrystalline materials with stress induced magnetic anisotropy $Fe_{73.5-x}Cr_xSi_{13.5}B_9Nb_3Cu_1$ (x = 1, 2, and 3) were selected. Although we did not expect a big difference in the properties of the nanocrystalline ribbons of these compositions, the above mentioned choice was adequate for demonstrating the stability of stress distribution by direct X-ray measurements using such a set of samples with Cr.

The ribbons were obtained in an amorphous state by single roller rapid quenching technique in the shape of ribbons with a cross-section of about 0.8 mm × 0.020 mm. The amorphous samples of each composition were subjected to heat treatment either without stress (conventional annealing, CA) or in presence of tensile stress, σ = 150 MPa (stress annealing, SA). In both cases the temperature of the heat treatments was 520 °C for time interval of 2 h. Table 1 lists all studied samples. The conditions of the heat treatments were selected taking into account previous studies of the classic and chromium doped FINEMET material: the temperature region of transition from amorphous to nanocrystalline state with nanograins happens in the region of about 510–570 °C [8,19].

Standard X-ray diffraction (XRD) data were collected on a Bruker D8 Advance diffractometer equipped with a Cu tube, Ge(111) incident beam monochromator (λ = 1.5406 Å) (fixed slit 1 mm) and a Sol-X energy dispersive detector (fixed slit 0.06 mm). The sample was mounted on a zero background silicon wafer embedded in a generic sample holder. Data were collected from 20° to 80° 2θ (step size = 0.05 and time per step = 65 s total time 22 h) at room temperature. A fixed divergence and antiscattering slits (1°) giving a constant volume of sample illumination were used.

Texture evaluation of the samples was performed using a Bruker D8 Discover diffractometer equipped with a Cu Twist tube, Ni filter (λ = 1.5418 Å), PolyCap™ (1μ single crystal cylinders) system for parallel beam generation (divergence of 0.25°), and a 1-D LynxEye detector (active length in 2θ 3°). The sample was mounted on an Eulerian Cradle with automatic controlled X–Y–Z stage. Data were collected for (110), (200) and (211) reflections at 44.87°, 65.63° and 83.38° in 2θ, respectively (using a fixed mode and time per orientation of 20 s). The data collection in standard mode was measured for full circle 0–360° increment 5° in Phi (ϕ) and 0–75 increment 5° in Psi (ψ) range giving 3456 total orientations.

Texture analysis using X-ray diffraction has typically been performed with the help of pole figure measurement. Such studies were performed by measuring exact 2θ maxima and rocking the sample through Psi (tilt) angles and Phi (spindle) rotations via a texture Cradle attachment. The measured intensities were then plotted as an intensity map where the hemisphere-like distribution of scattered intensity is projected on a 2D "pole figure" showing the variation of intensity with sample orientation. Each crystallite in a polycrystalline aggregate has a crystallographic orientation defined in a sample-defined referential. Pole figures are used to describe the variation in the pole density with pole orientation for a selected set of (hkl) crystal planes. A point on the "pole figure" corresponds to an orientation of the diffraction vector (normal to the diffracting plane) in a coordinate system fixed to the sample. The pole density for a given point is determined by the intensity of the X-ray beam diffracted for this orientation.

Residual stress of materials was tested using a Bruker D8 Discover diffractometer equipped with a Cu tube, Ni filter (λ = 1.5418 Å), Polycap system (divergence of 0.25°), 1 mm PinHole collimator for the incident beam and a 1-D LynxEye detector. The sample was mounted on an Eulerian Cradle with X–Y–Z stage. Data were collected from 116 to 121° 2θ (step size = 0.04 and time per step = 10 s). Strain values in side inclination mode were recorded for different sample tilt angles (Psi) seven steps, 0–0.7 range in $\mathrm{Sin}^2\psi$ (0°, 9.47°, 18.93°, 28.40°, 37.86°, 47.32° and 56.79°) at constant azimuth angles (phi). Strain vs. $\mathrm{Sin}^2\psi$ was plotted to estimate the stress values. In order to acquire a complete evaluation, at least six measurements on strain-$\mathrm{Sin}^2\psi$ plot using three different values of (Phi). 0°, 45°, and 90° were chosen in negative and positive values.

The hysteresis loops M(H) of the samples were measured by the inductive technique under application of an external magnetic field in plain of the ribbon and along the long ribbon side. Such magnetic parameters as coercivity (H_c), anisotropy field (H_a) and the induced magnetic anisotropy constants were deduced as the magnetization work [14] from the magnetization curves measured by a fluxmetric method [15]. K_u values were calculated with 5% error. For each composition the maximum induction (B_{max}) was calculated from the hysteresis loops measured by vibrating sample magnetometer (VSM) in the field 142 kA/m field (high enough to reach the magnetic saturation state). The obtained maximum values of induction (B_{max}), most important technological characteristic requested by applications, were in good agreement with the previously published data [19], confirming the quality of fabricated material: for $Fe_{73.5-x}Cr_xSi_{13.5}B_9Nb_3Cu_1$ samples B_{max} = 1.19, 1.08 and 0.95 T for x = 1, 2, and 3 accordingly.

3. Results and discussion

Although some data on magnetic and structural properties of FeCrSiBNbCu alloys were reported in the literature [8,19] the only way to prove the essential role of the anisotropic stress distribution is to evaluate carefully all possible contributions: grain size, texture, induced magnetic anisotropy constant value and anisotropic stresses. We therefore report careful analysis of the grain

Table 1
Description of the $Fe_{73.5-x}Cr_xSi_{13.5}B_9Nb_3Cu_1$ (x = 1, 2, and 3) samples, their selected properties: H_a – anisotropy field, H_c – coercivity, K_u – induced magnetic anisotropy constant; principal stress tensor components σ_I, σ_{II} and ±δ – the accuracy of the stress tensor components definition.

Sample	Cr (%)	Annealing	H_a (A/m)	H_c (A/m)	K_u (J/m^3)	σ_I (MPa)	σ_{II} (MPa)	±δ (MPa)
CA-I	1	Conventional 520 °C, 2 h	100	5 ± 1	~20	−39.5	40.8	11.7
SA-I	1	Stress 520 °C, 2 h	3100	3 ± 1	1900	307.0	46.4	11.1
CA-II	2	Conventional 520 °C, 2 h	100	5 ± 1	~20	−60.4	4.4	8.9
SA-II	2	Stress 520 °C, 2 h	3100	3 ± 1	1800	323.5	6.9	9.3
CA-III	3	Conventional 520 °C 2 h	100	5 ± 1	~20	−28.0	10.3	9.7
SA-III	3	Stress 520 °C 2 h	3000	3 ± 1	1700	364.4	82.9	11.1

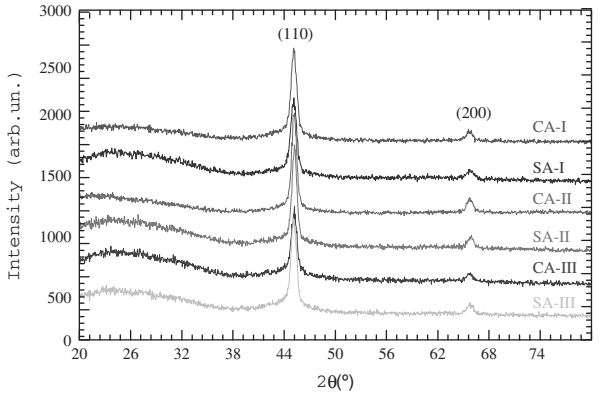

Fig. 1. Standard X-ray diffraction spectra of $Fe_{73.5-x}Cr_xSi_{13.5}B_9Nb_3Cu_1$ nanocrystalline ribbons with Cr content (x = 1%, 2%, and 3%): CA – conventional annealing, SA – stress annealing.

size, texture and induced magnetic anisotropy in order to extract corresponding part of the anisotropic stresses.

Fig. 1 shows conventional X-ray diffraction spectra for all nanocrystalline samples. Preliminary identification of the initial phases was evaluated using the Powder Diffraction File (PDF) database. XRD data were in good agreement with cubic bcc structure (00-037-0474), the fixed position (45.178° 2θ) for the first reflection (1 1 0) in all the samples was used to calculate a general unit cell parameter 2.836 Å (Fig. 2). X-ray diffraction has been widely used to determine crystallite size of FINEMET type materials [9,13]. Traditionally, the crystal size can be determined accurately based on the peak width of the principal XRD peak using the Scherrer formula:

$$\beta_{hkl} = 0.9 \cdot \lambda / L_{hkl} \cdot \cos\theta \quad (1)$$

where β_{hkl} is the broadening of the diffraction line measured at half the line maximum intensity (FWHM) (instrumental contribution was β_{Inst} = 0.08°), λ is the X-ray wavelength, L_{hkl} is the crystal size and θ is the diffraction angle. No significant differences were observed for the obtained crystallite size (about 13 nm) for all samples under consideration (Table 2).

Fig. 2 shows an example of texture analysis via the use of pole figure measurement with and without background correction. The measured intensities show low density signal in the pole figures perhaps as a result of an experimental artifact, nevertheless the obtained pole figures using no background correction represent typically not textured samples. The simulations proceeded using the Multex 3 software allows us to quantify the experimental error in less than a texture component equivalent to a 3%. These results indicated that the crystal orientations are close to be isotropic in good agreement with the results previously reported for example by Kraus et al. [16].

Based on the scale (at structural level) on which residual stresses in a polycrystalline material are constant, a classification of three types of residual stresses: 1st, 2nd and 3rd order, has been established by Macherauch et al. [21]. The 1st order residual stresses (σ^{I}_{rs}) are also called macroscopic residual stresses. They represent the mean stress value of all grains (crystals) in a macroscopic volume element. The 2nd order residual stresses (σ^{II}_{rs}) are defined as the stress average within an individual grain. The 3rd order residual stresses (σ^{III}_{rs}) vary on an atomic scale and they are caused by dislocations etc. The stress evaluation in this work using LEPTOS is mainly focusing on residual stresses of the 1st order, macroscopic stresses which cause an angular line shift of a measured diffraction peak. Therefore, X-ray diffraction could be used to estimate the residual stress of crystalline materials in a non-destructive way. Stress is evaluated from strain values using Young's modulus, Poisson's ratio and taking into consideration the elastic anisotropy of the materials.

The stress measurements using the X-ray diffraction are basically strain measurements in crystalline regions: the stresses can be calculated from the measured strains when the elastic constants are known. In a polycrystalline material with many crystals in random orientations a measuring vector $n_{\psi\varphi}$ must be introduced, describing the orientation of an experimental selected {hkl}-net-plane normal with respect to the sample coordinate system, by the azimuth angle φ(phi) and a tilt angle ψ(Psi). Obviously the strain $\varepsilon_{\psi\varphi}$ (in direction of $n_{\psi\varphi}$) also depends on the azimuth and tilt angles.

The procedure for stress measurements in a polycrystal can be performed by changing the tilt angle at a constant azimuthal angle, when the measured strains are plotted vs. $\mathrm{Sin}^2\psi$, X-ray stress analysis can be performed. The traditional Strain-$\mathrm{Sin}^2\psi$ method [22] is based on the elastic theory of an isotropic solid, which depends on the linear relation of measured diffraction strain ε and $\mathrm{Sin}^2\psi$, where ψ is the tilt angle of specimen (i.e. the inclination of the lattice–strain measurement direction with respect to the direction normal to the surface of specimen). The stress can be obtained from the slope of the straight line fitted to the measured ε – $\mathrm{Sin}^2\psi$ plot. The linear relation of ε and $\mathrm{Sin}^2\psi$ is effective for the analysis of a homogeneous stress state in a macroscopically isotropic elastic specimen. Positive values of stress indicate tensile stress and negative values compressive stress.

Stress has been evaluated from strain values using Young's modulus E (161 GPa), Poisson's ratio ν (0.320) and an elastic anisotropy Arx of 1.49 for Cubic body-centered Fe-base materials [17,23], taking into consideration, that X-Ray Elastic Constants s1 and ½ s2 are defined as: s1 = $-\nu/E$ and ½ s2 = $(\nu + 1)/E$, for a specific {hkl} reflection, (XECs) [24,25].

A single peak (3 1 0), available at the highest value of 2θ, was used for the analysis. The obtained results were adjusted using Leptos 7.03 software from Bruker AXS GmbH. The data were corrected for absorption, background (five points at edges), polarization, smooth and $K_{\alpha 2}$ subtraction, the peak evaluation was fitted by the Pearson VII function.

The determined ε – $\mathrm{Sin}^2\psi$ function using a biaxial model (linear function) without Psi splitting due to the shear stress component are shown in Fig. 4. The obtained results clearly indicate two very different stress behaviors for the samples after conventional and stress annealing (Table 1 and Figs. 3 and 4) showing very small dependence on the composition for the $Fe_{73.5-x}Cr_xSi_{13.5}B_9Nb_3Cu_1$ (x = 1, 2, and 3) alloys. For simplicity we analyzed in more detail the values of the stresses induced in the longitudinal, i.e. along the ribbon axis (σ_I stress tensor component) and transverse (σ_{II} stress tensor component) directions. The distribution of the stresses for CA and SA types of samples were very different and in perfect correlation with the results of magnetic measurements.

Fig. 5 (see also Table. 1) shows that FeCrSiBNbCu nanocrystalline ribbons after conventional annealing have longitudinal magnetic anisotropy with an easy magnetization axis oriented in plane of the ribbon and parallel to the long side of the ribbon. J is the vector field related to magnetization, M, as $M = J/\mu_0$, where μ_0 is the vacuum permeability. J_s is the vector field related to saturation magnetization. The observed coercive force was of the order of 5 ± 1 A/m for all CA samples. Nanocrystalline ribbons after stress annealing were characterized by the transverse magnetic anisotropy with an easy magnetization axis oriented in plane of the ribbon and perpendicular to the long side of the ribbon and the stress applied during the annealing. The observed coercive force was 3 ± 1 A/m for all SA samples. The value of the transverse magnetic anisotropy constant was of the order of 1800 ± 50 J/m^3 showing slight decrease with an increase of the chromium content.

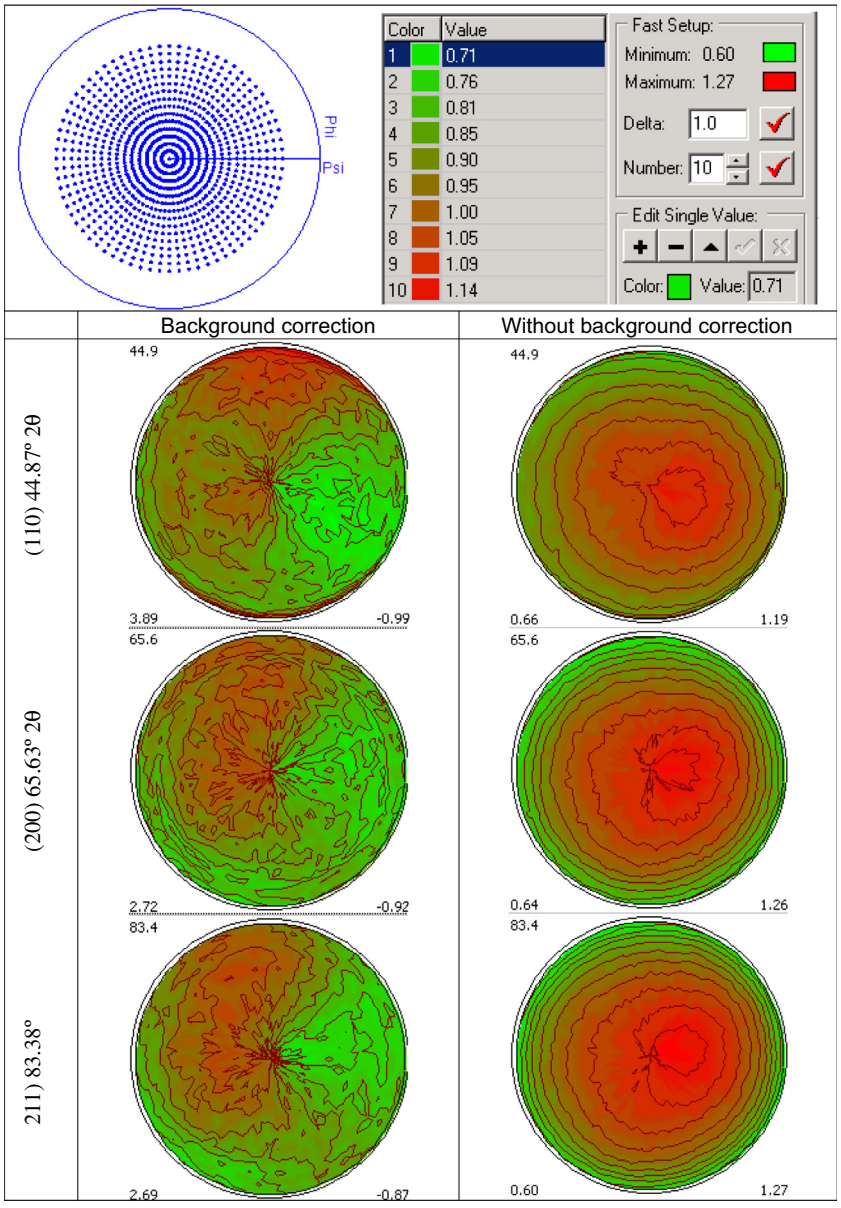

Fig. 2. Pole figures for SA-I stress annealed $Fe_{72.5}Cr_1Si_{13.5}B_9Nb_3Cu_1$ nanocrystalline ribbon showing no significant variation of intensity with sample orientation (no texture).

Table 2
Crystal size of the samples determined by XRD using of Scherrer Eq. (1).

Sample	Left angle 2θ (°)	Right angle 2θ (°)	Obs. max 2θ (°)	d (Obs. max) (Å)	FWHM 2θ (°)	B struct. 2θ (°)	Crystallite size (nm)
CA-I	40.650	48.900	45.120	2.00782	0.803	0.723	12 ± 2
SA-I	40.650	48.900	45.120	2.00783	0.822	0.742	12 ± 2
CA-II	40.650	48.900	45.181	2.00527	0.676	0.596	14 ± 2
SA-II	40.650	48.900	45.202	2.00438	0.682	0.603	14 ± 2
CA-III	40.650	48.900	45.181	2.00526	0.783	0703	12 ± 2
SA-III	40.650	48.900	45.115	2.00802	0.811	0.731	12 ± 2

For all CA samples (Figs. 3 and 4) with almost negligible induced magnetic anisotropy constant ($K_u \sim 20$), the following relation was observed: $\sigma_I \sim \sigma_{II}$, i.e. showing the tendency of the isotropic stress distribution. For all SA samples (Figs. 4 and 5) with $K_u \sim 1800$ J/m^3 the following relation was observed $\sigma_I \gg \sigma_{II}$, i.e. showing the tendency of the anisotropic stress distribution with much larger residual stress for the stress tensor component measured in the direction of the stress applied during stress annealing. One of the possible microscopic mechanisms responsible for such behavior can be the change of the spacing for crystallographic planes normal to the tensile direction of applied stresses in comparison with the ones parallel to it like it was observed in [15] or discussed in [13]. In any case the stress tensor anisotropy in the conditions of the same size of the nanocrystals (of about 13 nm) and absence of crystallographic texture (proven by pole figures analysis) for approximately the same induced magnetic anisotropy value seems to be

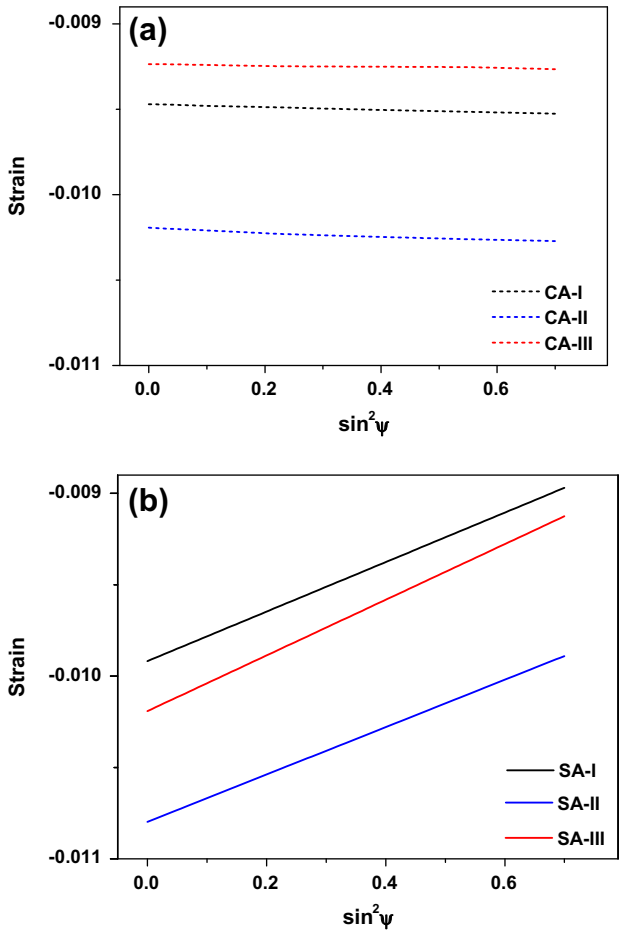

Fig. 3. Strain – $Sin^2\psi$ function fit for all conventionally annealed $Fe_{73.5-x}CrxSi_{13.5}B_9Nb_3Cu_1$ nanocrystalline ribbons with chromium ($x = 1\%$, 2%, and 3%) for the ribbon axis (a). Strain – $Sin^2\psi$ function fit for all stress annealed $Fe_{73.5-x}Cr_xSi_{13.5}B_9Nb_3Cu_1$ samples for the ribbon axis (b).

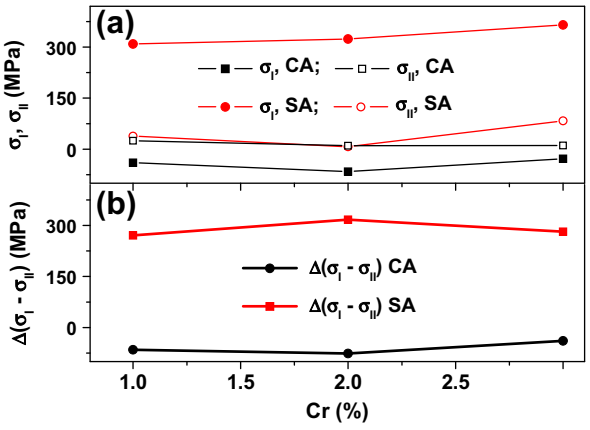

Fig. 4. Summary of the analysis of stress distribution for $Fe_{73.5-x}Cr_xSi_{13.5}B_9Nb_3Cu_1$ nanocrystalline ribbons with chromium content ($x = 1\%$, 2%, and 3%): (a) σ_I and σ_{II} components of stress tensor and (b) difference between σ_I and σ_{II} components for all samples listed in Table 1.

an argument that supports the point of view that anisotropic stress distribution is the primary source of induced magnetic anisotropy in the case under consideration.

One should also discuss stress distribution features as a function of chromium content (Figs. 3 and 4). Taking into account the

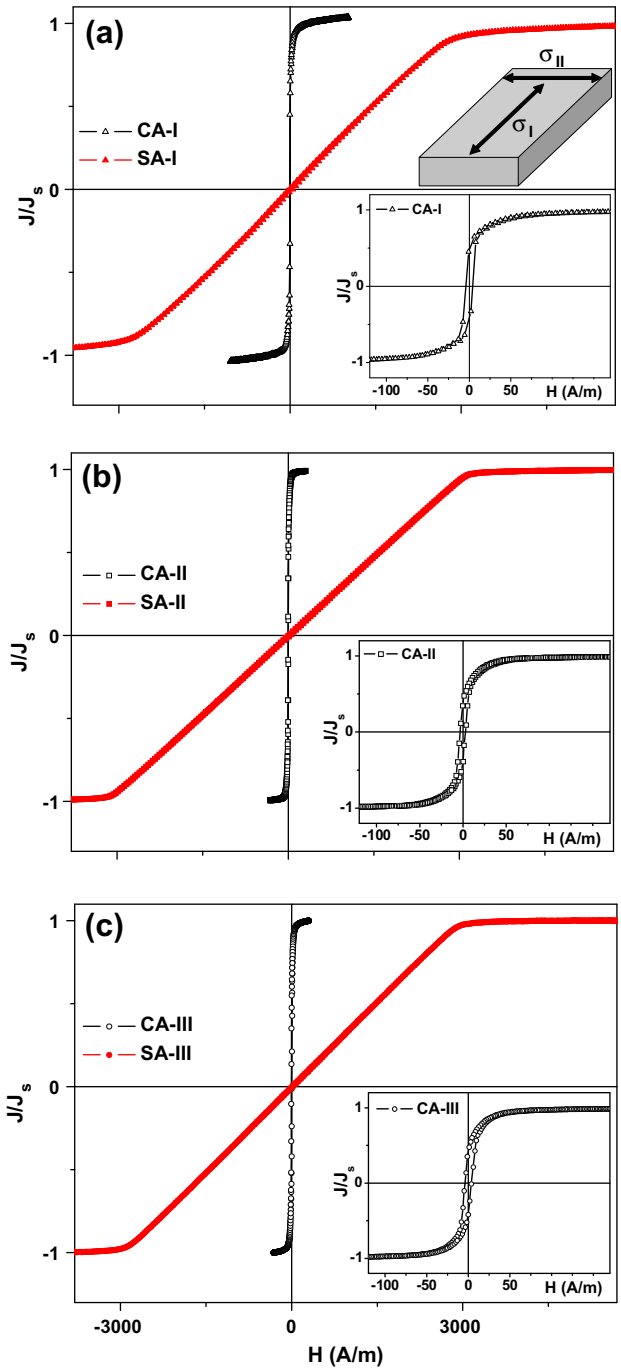

Fig. 5. Inductive hysteresis loops for $Fe_{73.5-x}Cr_xSi_{13.5}B_9Nb_3Cu_1$ nanocrystalline ribbons with different Cr content ($x = 1\%$, 2%, and 3%) (see also Table 1) after conventional and stress annealing. Insets show low field parts of the hysteresis loops.

accuracy of the stress tensor components definition we came to the conclusion, that σ_I and σ_{II} components of stress tensor show a rather weak dependence on the chromium content for the composition range under consideration. At the same time, close values of corresponding σ_I and σ_{II} components serve as confirmation of the possibility to establish repetitive procedure of X-ray stress tensor measurements in reflection mode for the case of single amorphous ribbon sample.

We have shown that accurate stress tensor measurements by X-ray technique in combination with conventional XRD studies can be used as an additional powerful non-destructive tool for

investigating structural peculiarities of nanocrystalline soft magnetic materials in the shape of ribbons with a guarantee of satisfactory results even in the case of very brittle materials.

4. Conclusion

The structure and magnetic properties of $Fe_{73.5-x}Cr_xSi_{13.5}B_9Nb_3Cu_1$ (x = 1, 2, and 3) alloys were comparatively studied in detail. Conventional annealing at 520 °C for 2 h resulted in longitudinal magnetic anisotropy formation with $K_u \sim 20\ J/m^3$. Stress annealing at 520 °C for 2 h for the specific load of 150 MPa resulted in the formation of the transverse induced magnetic anisotropy with the K_u constant of the order of $1800\ J/m^3$. No significant differences for the obtained crystallite size (about 13 nm) were observed for all samples. The crystallite orientations were practically isotropic indicating no texture in the samples of all types. For all CA samples with $K_u \sim 20\ J/m^3$ a $\sigma_I - \sigma_{II}$ relation was observed showing a tendency of the isotropic stress distribution. For all SA samples with $K_u \sim 1800\ J/m^3$ σ_I was much higher than the σ_{II}: the tendency of the anisotropic stress distribution was observed indicating an important role of anisotropic stress distribution in the stress induced magnetic anisotropy formation. Stress tensor measurements by X-ray technique can be used as an additional powerful non-destructive tool for investigating structural peculiarities of nanocrystalline soft magnetic materials.

Acknowledgments

This work was supported by Etortek Actimat grant of the Basque Government and UPV-EHU, URFU 215 grant and partly by the Presidium of RAS (pr. 12-II-23-2005) and RFBR NO 12-02-31385 grant. The authors thank A.P. Potapov for special support. Selected measurements were done in SGIKER Services, UPV-EHU.

References

[1] Y. Yoshizawa, S. Oguma, K. Yamauchi, J. Appl. Phys. 10 (2) (1988) 6044–6046.
[2] G. Herzer, Encyclopedia of materials science and technology, in: K H J Buschow Amsterdam (Ed.), Elsevier, 2001, p. 149.
[3] M. Vazquez, G.V. Kurlyandskaya, J.M. Garcia-Beneytez, J.P. Sinnecker, J.M. Barandiaran, V.A. Lukshina, A.P. Potapov, IEEE Trans. Magn. 35 (5) (1999) 3358–3360.
[4] P. Allia, M. Baricco, P. Tiberto, F. Vinai, Kinetics of the amorphous-to-nanocrystalline transformation in Fe73.5Cu1Nb3Si13.5B9, J. Appl. Phys. 74 (5) (1993) 3137–3143.
[5] V.M. Prida, P. Gorria, G.V. Kurlyandskaya, M.L. Sanchez, B. Hernando, M. Tejedor, Nanotechnology 14 (2003) 231–238.
[6] A.V. Semirov, D.A. Bukreev, A.A. Moiseev, S.O. Volchkov, G.V. Kurlyandskaya, V.A. Lukshina, E.G. Volkova, Temperature dependences of magnetoimpedance of nanocrystalline Fe-Based ribbons, J. Nanosci. Nanotechnol. 12 (2012) 7446–7450.
[7] N. Chau, P.Q. Thanh, N.Q. Hoa, N.D. The, J. Magn. Magn. Mater 304 (2006) 36–40.
[8] A. Zeleňáková, J. Füzer, P. Kollár, M. Kužminski, J. Magn. Magn. Mater. 304 (2006) e528–e530.
[9] M.E. McHenry, M.A. Willard, D.E. Laughlin, Prog. Mater. Sci. 44 (1999) 291–433.
[10] G. Chen, X.L. Yang, L. Zeng, J.X. Yang, F.F. Gong, D.P. Yang, Z.C. Wang, J. Appl. Phys. 87 (9) (2000) 5263–5265.
[11] B. Hofmann, H. Kronmuller, J. Magn. Magn. Mater. 152 (91) (1996) 91–98.
[12] G. Herzer, IEEE Trans. Magn. 30 (1994) 4800–4802.
[13] N.V. Ershov, N.V. Dmitrieva, Yu.P. Chernenkov, V.A. Lukshina, V.I. Fedorov, A.P. Potapov, Sol. State. Phys 54 (9) (2012) 1817–1826.
[14] S.J. Kernion, P.R. Ohodnicki, J. Grossmann, A. Leary, Sh. Shen, Vladimir Keylin, J.F. Huth, J. Horwath, M.S. Lucas, M.E. McHenry, Appl. Phys. Lett. 101 (2012) 102408.
[15] M. Ohnuma, K. Hono, T. Yanai, H. Fukunaga, Y. Yoshizawa, Appl. Phys. Lett. 83 (14) (2003) 2859–2861.
[16] L. Kraus, K. Závta, O. Hesco, P. Dujaj, G. Vlasák, J. Schneider, J. Magn. Magn. Mater. 112 (1992) 275–277.
[17] M. Ohuma, K. Hono, T. Yanai, M. Nakano, H. Fukunaga, Y. Yoshizawa, Appl. Phys. Lett. 86 (2005) 152513.
[18] Yu.P. Chernenkov, N.V. Ershov, V.I. Fedorov, V.A. Lukshina, A.P. Potapov, Phys. Sol. State 52 (2010) 554–560.
[19] V.A. Lukshina, N.V. Dmitrieva, M.A. Cerdeira, A.P. Potapov, J. Alloys. Comp. 536 (Suppl. 1) (2012) S374–S377.
[20] G.V. Kurlyandskaya, A. Garcia-Arribas, J.M. Barandiaran, E. Kisker, Sens. Actuators A 91 (2001) 116–119.
[21] E. Macherauch, H. Wohlfahrt, U. Wolfstieg, Härtereitechn. Mitteilungen 28 (1997) 201–211.
[22] P. Müller, E. Macherauch, Zeitschrift angewandte Physik 13 (1961) 305–312.
[23] LEPTOS Stress Database, DOC-M88-EXX052 V7, Bruker AXS GmbH (2009).
[24] A.C. Vermeulen, JCPDS-International Centre for Diffraction Data, Adv. X-ray Anal. 44 (2001) 128–133.
[25] V.M. Hauk, E. Macherauch, Adv. X-ray Anal. 27 (1983) 81–99.